

The Impact of Steel Microstructure and Heat Treatment on the Formation of White Etching Cracks

Benjamin Gould^{1*}, Mohanchand Paladugu², Nicholas G. Demas¹, Aaron C. Greco¹, R. Scott Hyde²

¹Applied Materials Division, Argonne National Laboratory Lemont IL

²The Timken Company World Headquarters (WHQ), North Canton, OH, 44720, USA

Abstract:

White etching crack (WECs) associated macro-pitting is a dominant mode of damage within wind turbine gearbox bearings. This damage is characterized by broadly branching crack networks surrounded by local regions of microstructural alterations. The definitive cause of WECs in the field is unknown; therefore, the implementation of effective mitigation techniques has proven difficult. The current work utilized an accelerated benchtop testing technique in order to quantify differences in performance between through-hardened AISI 52100 steel and carburized AISI 3310 steel. It was found that the carburized AISI 3310 steel demonstrated a more than twofold increase in the time elapsed until WEC macro-pitting damage occurred compared to the through-hardened AISI 52100 steel samples.

Key Words: White Etching Cracks; Bearing; Microstructural Alterations; Premature Fatigue; Carburization

Acknowledgments:

This work is supported by The Timken Company and the U.S. Department of Energy Office of Energy Efficiency and Renewable Energy, Wind Energy Technology Office under Contract No. DE-AC02-06CH11357. The authors are grateful to DOE Project Managers Mr. Michael Derby and Mr. Brad Ring for their support and encouragement. The authors would also like to acknowledge the assistance provided by our colleagues at Argonne National Laboratory's Tribology Section.

1.0 Background

Bearings used in large-scale drivetrain applications, particularly those of wind turbines, are often subjected to a wide range of operating conditions that sometimes result in spalling or macro-pitting well before the rolling contact fatigue (RCF) design life of the bearing [1–3]. Frequently, the cracks that lead to these catastrophic failures are surrounded by local areas where the bearing steel has undergone a microstructural alteration resulting in a nano-grained structure [4–8].

When bearings exhibiting this damage are metallurgically examined through a process of sectioning and etching with Nital (nitric acid and ethanol), the local nano-grained regions resist the etchant and appear white in contrast to the surrounding steel matrix. Because of its white appearance, this type of damage is often referred to as “white etching cracks” (WECs). Figure 1(a) shows a wind turbine bearing that has experienced macro-pitting damage caused by the WEC network shown in Figure 1(b).

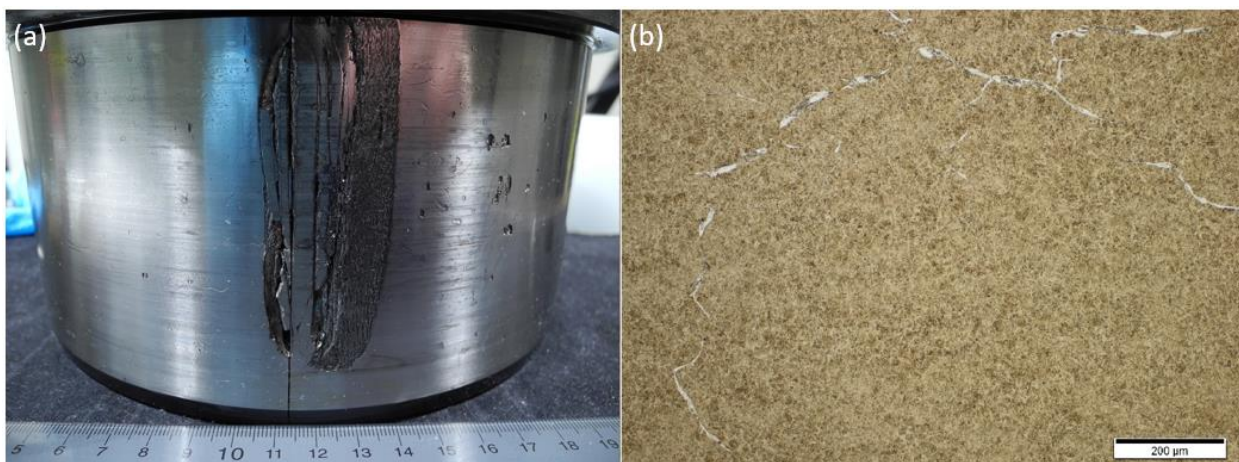


Figure 1. (a) A wind turbine bearing that has experienced macro-pitting damage; (b) a section of the crack shown in (a). Image taken from [9]

The exact conditions that lead to the formation of WECs in field bearings are unknown. Previous authors have attributed the root cause of the cracks to a variety of reasons, including applied strain due to normal loading [10–24], torque reversals leading to impacts [18,19,25], hydrogen release from degraded or contaminated lubricants [16,26,27], electrical discharge [28], tensile frictional stresses at the contact surface [29], and sliding contacts induced via acceleration or under-loading [30,31]. Because there is no consensus on the drivers of WEC formation in the field, multiple avenues have been followed to recreate these crack networks using accelerated benchtop tests. These efforts employed methods such as the use of specific lubricant formulations thought to aid in the formation of WECs [9,24,32–41], pre-charging test samples with hydrogen [42–57], grain boundary embrittlement induced via heat treatment [58], the application of external electrical load [28], excessive slip [9,24,59,60], and impact loading [61].

In-depth reviews of the leading hypotheses on the formation of WECs can be found in [17,62,63]. Recent work by Gould et al. [62,64] aimed to elucidate the drivers of WEC formation by performing synchrotron level X-ray tomography at the Advanced Photon Source (APS) research facility in order to map and study the morphology of WECs within damaged field bearings. Their research found that the WEC networks studied initiated in the subsurface of the bearings, preferentially at inclusions that contained both a manganese sulfide component and an aluminum oxide component. Additionally, the work by Gould et al. [64] identified the formation of the crack as a prerequisite to the formation of the white etching areas (WEAs) adjacent to the crack faces. This suggests that efforts to mitigate WECs should aim at diminishing both the rate at which cracking forms around inclusions and the rate at which these cracks propagate, with the formation of white etching matter surrounding the cracks as a secondary effect.

One method commonly employed to mitigate the formation of cracking is the use of carburization [65,66]. Carburization refers to a process in which carbon is diffused into the outer layer of hypo-eutectoid steels, thus resulting in a microstructure that varies with depth. After heat treatment, the outer layer of the steel transforms into a high-hardness shell with an inherent compressive residual stress. The core of the sample, which does not contain any diffused carbon, maintains a relatively soft microstructure and high toughness. Although the process of carburization incurs additional costs, if done correctly, the compressive residual stress induced in the shell, in combination with the higher toughness of the core, can combat crack initiation, propagation, and fatigue damage [67]. Additionally, previous research has indicated that the use of carburized bearing, particularly those with over 20% retained austenite (RA) maybe especially effective at mitigating the formation of WECs [68].

The aim of the current work was to quantify if the process of carburization affects the rate at which cracks containing local WEAs manifest within bearing steel. This was done by applying a previously developed set of benchtop test conditions in conjunction with a WEC accelerating lubricant [9,24] to test samples consisting of two different microstructures. The first set consisted of AISI 52100 steel samples that had undergone a through-hardening process; the second set of samples instead was made of carburized AISI 3310 steel. The authors hypothesize that the use of the carburized AISI 3310 steel will prolong the time until the formation of a macro-pit due to the fact that the induced compressive residual stress associated with the carburization will help prevent both crack initiation and propagation.

2.0 Methods

All tests within this study were performed on the PCS Instruments micro-pitting rig (MPR) shown in Figure 2(a). The MPR utilizes a three-ring-on-roller (Figure 2(b)) contact

configuration that is splash lubricated and can be operated at various conditions ranging from pure rolling to pure sliding, at stresses up to 4 GPa, at temperatures in excess of 100°C and at speeds of up to 4 m/s resulting in approximately 300 contacts per second. This test rig and lubricant have been used in multiple studies examining the formation of WECs, most notably in [9,24,39,41]. These studies found that the load, lubrication condition, lubricant formulation, stress profile, test duration, and both the magnitude and direction of sliding had an effect on the formation of WECs.

The authors also correlated the formation of WECs to the cumulative energy a test sample had experienced [24]. It was hypothesized that the formation of WECs in these studies was caused by subsurface crack initiation followed by energy localization adjacent to the crack faces that resulted from the combination of crack-face rubbing caused by over-rolling and the large frictional energy imparted by the sliding contact.

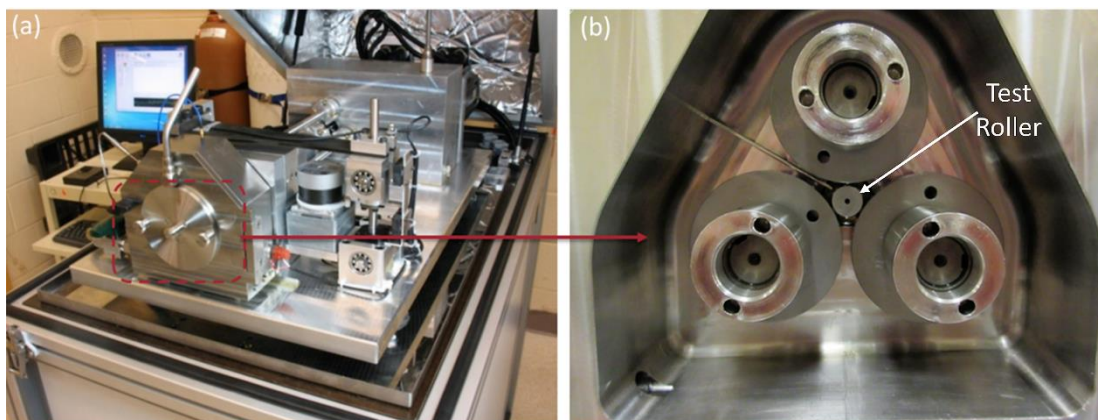


Figure 2. (a) The PCS Instruments micro pitting rig (MPR), which contains a three-ring-on-roller contact shown in (b), used to simulate rolling/sliding between a bearing roller and raceway. Image taken from [9]

The test specimens examined for WECs throughout the present work were 12 mm-diameter rollers, as shown in Figure 3. Each roller has a 1 mm-wide test track that comes into contact with each of the three 54 mm-diameter rings. Ten rollers consisting of two different steel microstructures were fabricated for the current study. One set of rollers consisted of AISI 52100

steel that had undergone a through-hardening heat treatment, and the second set of rollers were manufactured using AISI 3310 steel that had been subjected to carburization treatment. The elemental composition of the two steels is shown in Table 1. The use of these different steel types resulted in variances in multiple material properties including hardness, residual stress, and RA percentage.

Figure 4 shows graphs of the measured values of these three parameters as a function of depth below the contact surface for the two steel types. These values were obtained by sectioning and analyzing an untested sample of each of the steels. The values of surface and subsurface residual stress and retained austenite were measured using X-ray diffraction (XRD) tangential to the raceway surface. The raceway was electrochemically etched to the required depth before measuring by XRD, as described in the relevant ASTM standards [69,70]. Micro-hardness was measured using a CLARK Vickers micro-hardness tester at a load of 500 grams. The equivalent HRC values as a function of the depth below the surface are shown in Figure 4(a).

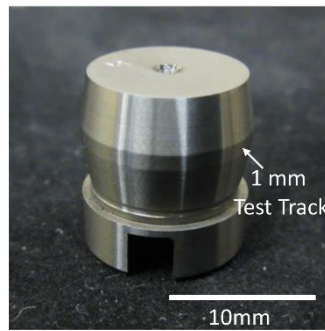


Figure 3. The 12mm diameter test roller used in the MPR; it is placed in the center of the three rings as shown in Figure 2(b). Image taken from [9]

Table 1. The elemental composition of the two steels studied in the current work

Element	AISI 52100 (wt%)	AISI 3310 (wt%)
Carbon (C)	1.02	0.12
Manganese (Mn)	0.32	0.4
Phosphorus (P)	0.015	0.008
Sulfur (S)	0.007	0.0016
Silicon (Si)	0.27	0.27

Chromium (Cr)	1.46	1.53
Nickel (Ni)	0.1	3.39
Molybdenum (Mo)	0.04	0.08
Copper (Cu)	0.19	0.22
Aluminum (Al)	0.026	0.03
Tin (Sn)	0.008	0.009
Vanadium (V)	0.003	0.009
Tungsten (W)	0.002	0.01
Niobium (Nb)	0.007	0.009
Iron (Fe)	Remainder	Remainder

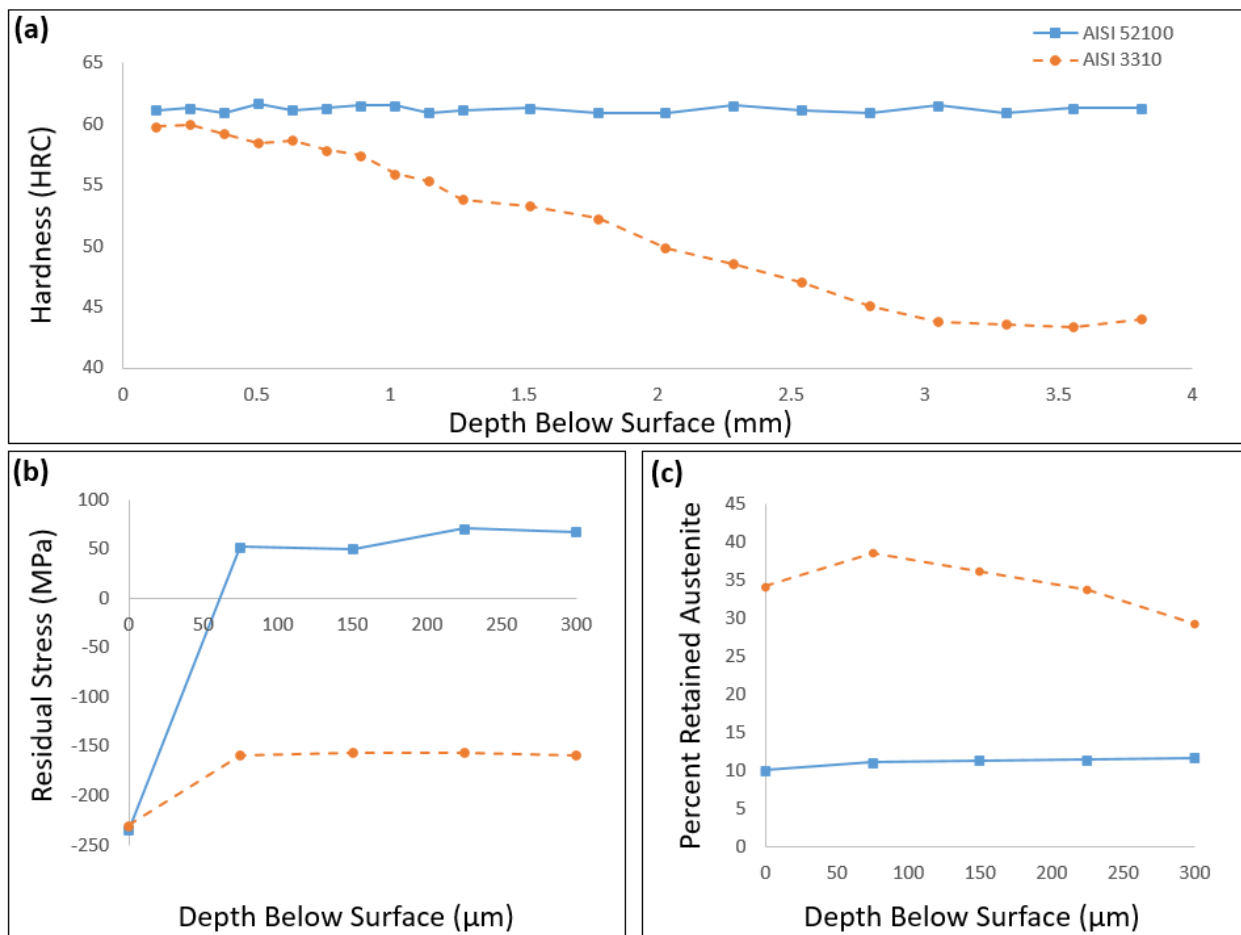


Figure 4. Measured values of the (a) hardness, (b) residual stress and (c) retained austenite vs. depth below the contact surface for the two steels studied in the current work

The lubricant used in this study was a semi-synthetic, viscosity grade (VG) 68, fully formulated gear oil. The metallic content of the oil was determined through inductively coupled plasma mass spectrometry (ICP-MS). All detected metals that returned quantities of greater than

1 ppm are shown in Table 2. This lubricant is known to contain both a zinc dialkyldithiophosphate (ZnDDP) compound and over-based calcium sulfonate (CaS), and has been referred to as a bad reference oil in numerous studies [6,6,36,60,71,72]. Additionally, it should be stated that this lubricant is not a commercial wind turbine gearbox oil.

Table 2. The metallic elemental composition of the gear oil used in the current work (all elements detected at levels greater than 1 ppm are shown)

Metal Detected	Quantity Detected
Sodium (Na)	>1000ppm
Boron (B)	720ppm
Zinc (Zn)	1970ppm
Phosphorus (P)	1698ppm
Calcium (Ca)	3811ppm
Magnesium (Mg)	8ppm
Potassium (K)	3ppm

Tests 1–8 were conducted under identical conditions in order to investigate whether material composition and heat treatment have an effect on the formation of WECs. These conditions were selected because they have previously been shown to lead to repeatable WEC formation. Tests 9 and 10 were conducted after analysis was performed on Tests 1–8. The objective of these tests was to study the initiation point of WECs within both steels, and they will be discussed in detail after the results of Tests 1–8 are presented.

All tests were conducted using identical parameters: 500N Load, -30% slide-to-roll ratio (SRR), 3.4m/s rolling speed, and 100°C. The presented test conditions resulted a maximum subsurface shear stress of 1.9GPa at a 125 μ m. The equation for calculating SRR in the MPR is shown in Eq. 1. Under these testing conditions, the roller acts as the driver, thereby having a faster interfacial velocity than the rings. Prior to each of the tests, the samples underwent a 30-minute run-in at a contact pressure of 1.9 GPa, -5% SRR and a rolling speed of 2 m/s. This set of conditions resulted in boundary lubrication with a lambda ratio of approximately 0.25. An accelerometer was used to monitor the vibration of the top ring throughout each test. Tests

stopped when a vibration level corresponding to the formation of significant surface damage – as demarcated by a specified significant increase in the vibration level – was detected.

$$SRR(\%) = \left(\frac{2 \cdot (U_{Ring} - U_{Roller})}{U_{Roller} + U_{Ring}} \right) \cdot 100 \quad \text{Eq. 1}$$

At the end of every test, the respective roller was sectioned in the circumferential depth plane. Samples were then mounted in Bakelite and polished to multiple locations along the wear track using a series of polishing steps: 220 grit (grinding) followed by 9 μm, 3 μm, and 1 μm diamond polishing media. At each section, the samples were etched with a 3% Nital solution in order to examine the subsurface for microstructural alterations. This process is illustrated in Figure 5.

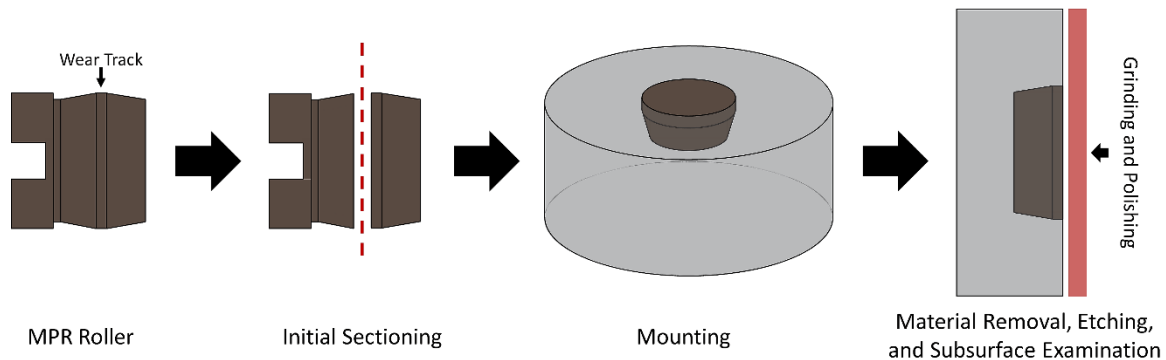


Figure 5. Optical microscope images of the wear track of an example roller showing the pitted surface (a) before sectioning and (b) after sectioning. The dotted red line represents the circumferential section that was taken in order to determine the presence of WECs

3.0 Results

Tests 1–8 all resulted in the formation of a macro-pit induced by crack networks surrounded by nano-grained microstructural alterations. Characteristic images of the macro-pits generated in each of the steel populations are shown in Figure 6. The specific number of contact cycles until a macro-pit formed for each test is shown in Table 3. The average number of contact cycles to the formation of a macro-pit (weibull L_{50} median life) with 65% confidence interval (corresponding to one standard deviation in failure rate) for each of the tested steels is shown in

Figure 7. On average, the carburized samples lasted ~2.3 times longer than the through-hardened samples. It is also worth noting that the carburized samples had a much larger variance in the number of cycles until macro-pit formation than the through-hardened samples. A two-tailed t-test was performed on the two data sets with the aim of quantifying if the AISI 3310 sample set significantly outperformed that of the AISI52100 samples. The test resulted in a P-value of 0.03, therefore it can be stated with over 95% confidence that the AISI 3310 sample set significantly outperformed that of the AISI 52100 samples with regard to the number of contact cycles until the development of a WEC induced macro-pit under the presented testing conditions.

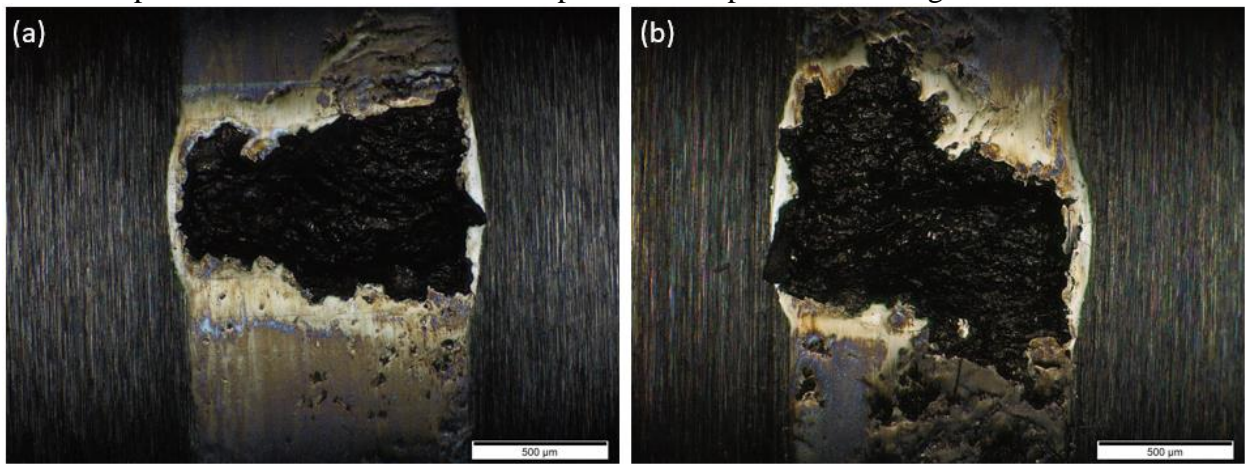


Figure 6 Optical characteristic images of the WEC induced macro-pits which led to the automatic shutdown of rollers in each steel population. (a) shows that of an AISI 52100 roller (Test 3) and (b) shows that of an AISI 3310 roller (Test 5)

Table 3. Testing conditions and test results for all 8 tests conducted in the presented study

Test #	Heat Treatment	Contact Cycles (10 ⁶)	Did The Sample Macro-pit	WECs Present?
1	T.H.	39.2	Yes	Yes
2	T.H.	49.1	Yes	Yes
3	T.H.	39.2	Yes	Yes
4	T.H.	37.4	Yes	Yes
5	C.C.	95.4	Yes	Yes
6	C.C.	56.0	Yes	Yes
7	C.C.	82.0	Yes	Yes
8	C.C.	145.2	Yes	Yes
9	T.H.	30.0	No	Yes

10 | C.C. 30.0 No Yes

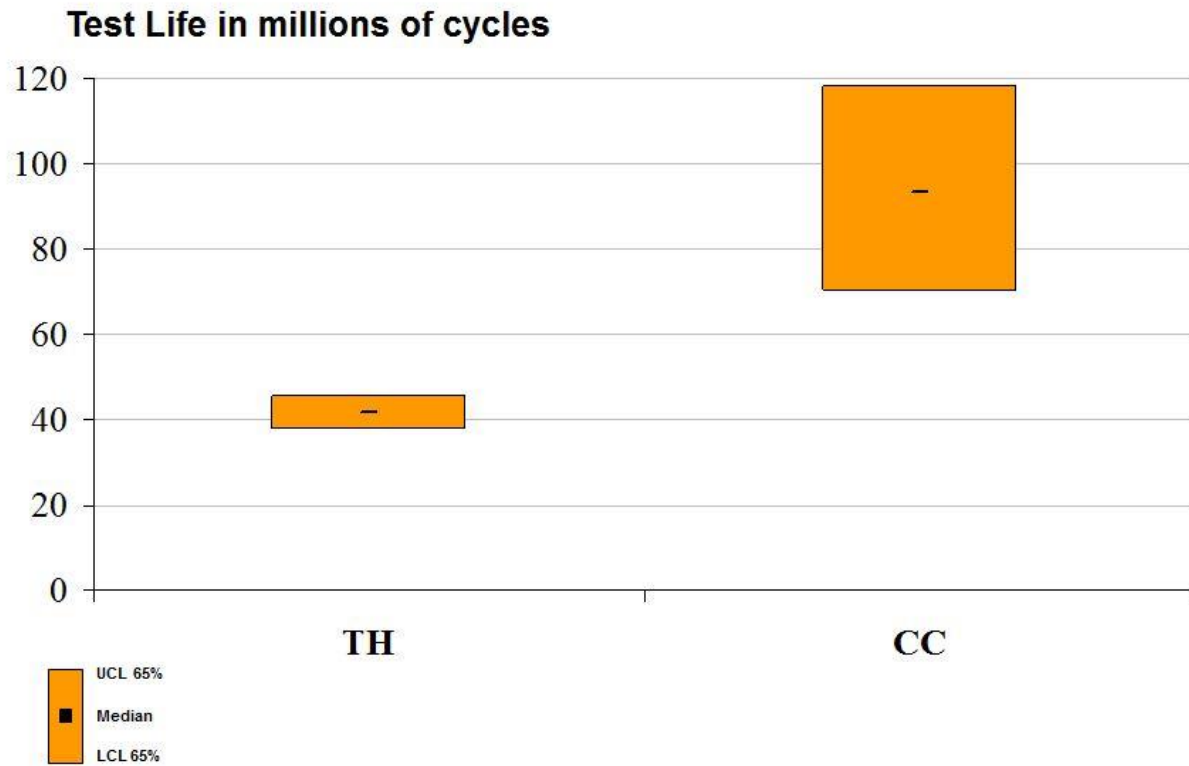


Figure 7. Weibull median life (L_{50}) with 65% confidence interval: a graph showing the difference in number of RCF cycles until the occurrence of WEC-induced damage for through-hardened samples (left) and carburized samples (right).

4.0 Discussion

As discussed above, the process of carburization results in a microstructure that varies in mechanical properties as a function of depth. The surface of a carburized sample is designed to be supersaturated with carbon in order to have a hardness similar to that of a through-hardened sample. However, the carbon content decreases as a function of depth below the surface; therefore, hardness decreases and toughness increases. This microstructure, in combination with the inherent compressive residual stress induced by the local carbon excess, resists crack formation and propagation [73,74].

In the samples used in the present work, the observed carburized layer was optically visible to a depth around 1 mm (as shown in Figure 8). Additionally, all the documented WECs seemed to initiate within the case layer. Therefore, the authors postulate that the major contributors to the prolonged time until macro-pit formation is the inherent compressive stress within the case layer, in combination with the increased toughness inherent in a microstructure resulting from carburization. Moreover, these results validate the idea that if steps are to be taken to prevent WEC formation, they should aim at mitigating the initiation and propagation of the crack itself as opposed to microstructural alterations which decorate it.

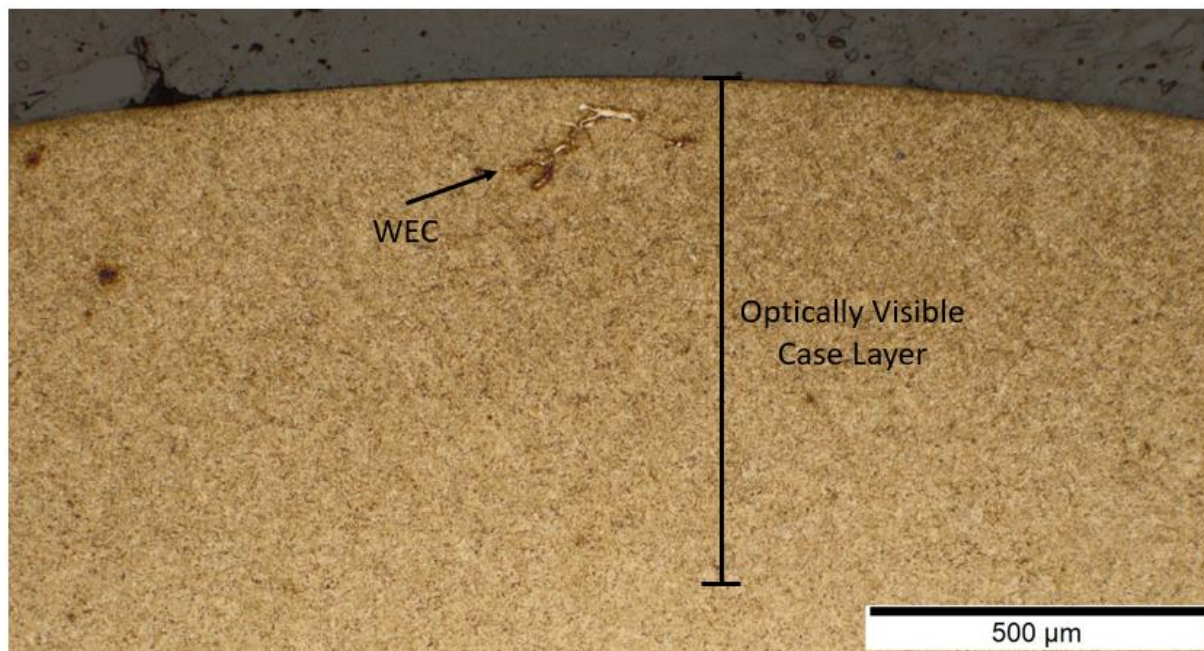


Figure 8. An etched optical image subsurface image of the roller used in Test 10 showing both the optically visible case layer (darker etching area) as well as a WEC clearly initiation and propagating within this case layer

4.1 Initiation vs. Propagation

The rate of macro-pit formation data shown in Figure 7 clearly illustrates that the AISI 3310 samples outperformed the AISI52100 samples with regards to number of contact cycles until the formation of a macro-pit. However, it is unclear from these eight tests if the AISI 3310 steel prolonged the time to crack initiation, the rate of crack propagation, or both. Tests 9 and 10

were conducted in an attempt to understand the point of crack initiation for both the AISI 3110 and the AISI 52100 samples. In these tests, an AISI 52100 and an AISI 3310 sample were both stopped and metallographically examined at 30 million contact cycles, well before the formation of a surface pit. WECs were observed in both Tests 9 and 10, characteristic examples of the WECs observed in Tests 9 and 10 are shown in Figure 9. Because WECs were observed in both Test 9 and 10, no difference in crack initiation point could not be documented. However, if it is assumed that the rollers from Tests 9 and 10 would fail close to the documented average for each steel set (94.65 and 41.23 million cycles for AISI 3310 AISI 52100 respectively) then it can be stated that the AISI 3310 steel significantly impedes the rate of crack propagation within rollers. This prolonged time of crack propagation is likely due compressive residual stress induced by the carburized microstructure, and the may be the main contributor to the longer observed life.

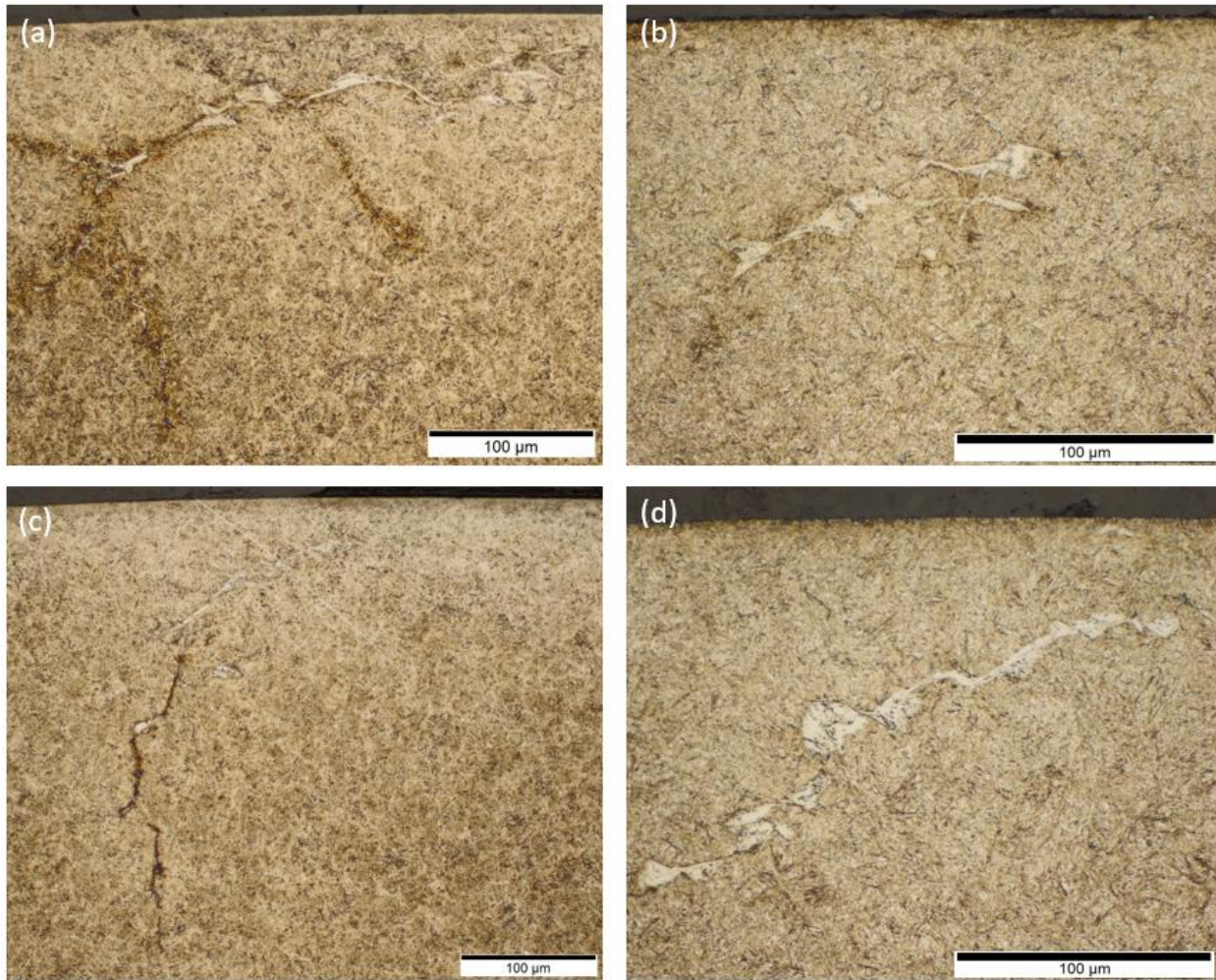


Figure 9 Characteristic examples of the WECs that were observed when an AISI 52100 sample (a and c) and an AISI 3310 sample (b and d) were both stopped at 30 million contact cycles (the images are oriented so the raceway is at the top of the page and the over-rolling direction is from the left to the right)

4.2 Differences in Morphology

Throughout the metallurgical examination of the 10 samples discussed in the current work, the authors observed some systematic differences in the morphology of both the crack networks and the WEAs that accompany them. First, the through-hardened AISI 52100 samples showed far more instances of vertical crack propagation than the case-carburized AISI 3310 samples. This observation falls in line with previous analysis on field bearings which stated that WEC damage in TH samples tends to manifest as axial cracking while WEC damage in CC

samples manifests as macro-pits [68]. An example showing this difference in morphology can be seen in Figure 10. Vertical crack propagation has been well documented in both field and benchtop-generated WECs [9,24,62–64,75,76]. In the field, this cracking is normally attributed to induced hoop stress caused by the bearing mounting or tensile residual stress from the heat treatment. However, there is no hoop stress in the manufactured MPR samples, since they are not mounted via a through-hole. Therefore, it is possible that subsurface residual stress, in combination with the induced contact stresses, could lead to this vertical cracking. In such a case, it is expected that the AISI 52100 steel would be more susceptible to vertical cracking than the AISI 3310 because its residual stress becomes tensile at a depth of $\sim 100\ \mu\text{m}$, while the AISI 3310 maintains a compressive residual stress until at least a depth of $300\ \mu\text{m}$ (see Figure 4(c)).

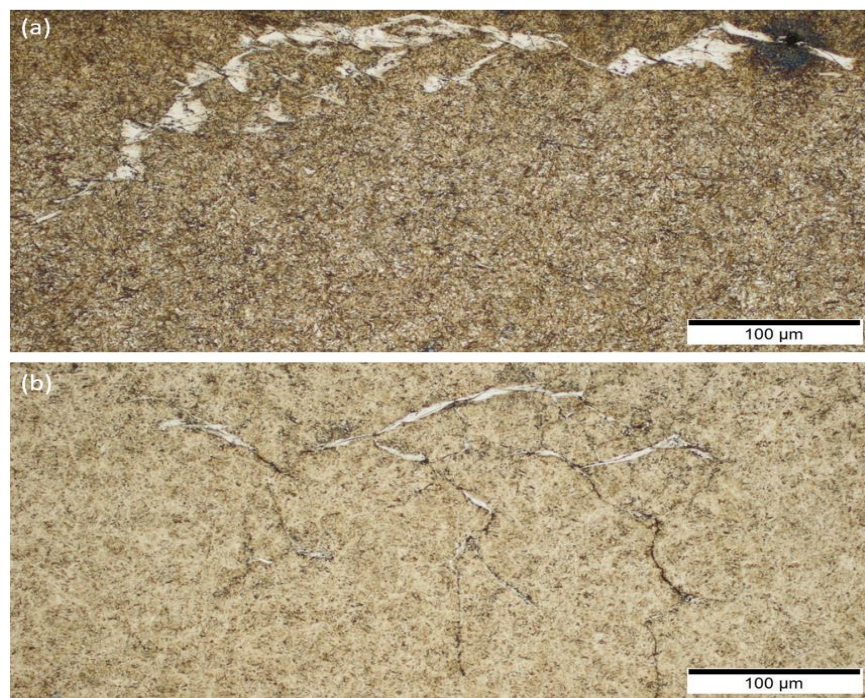


Figure 10. Two WEC networks found in the two different steel types (the images are oriented so the raceway is at the top of the page and the over-rolling direction is from the left to the right): (a) A WEC network found within the case-carburized AISI 3310 samples; (b) a WEC network found within the through-hardened AISI 52100 samples. The crack network in (b) shows far more instances of vertical crack propagation than that in (a)

It was also observed that the width of the WEAs that accompanied the cracks within the carburized samples appeared larger than the WEAs that accompanied the cracks within the through-hardened samples. Examples of this observation are shown in Figure 11. The width of a WEA adjacent to a crack face can be viewed as an indicator of the magnitude of energy that has been released in a local area. Because it is assumed that that the crack is a prerequisite to the formation of the WEA [24,63,64], and the test conditions are constant, the authors have two hypotheses as to why the carburized samples exhibit larger regions of WEA.

The first hypothesis is that the microstructure of the AISI 3310 samples led to a significant decrease in the rate of crack propagation, as discussed in the previous section; therefore, the cracks in these samples underwent a significantly larger number of contact cycles and accrued a larger amount of localized energy. The second hypothesis is that the inherent compressive residual stress in the carburized samples may have led to an increase in the amount of crack-face rubbing and, therefore, an increase in the frictional energy released by the crack.

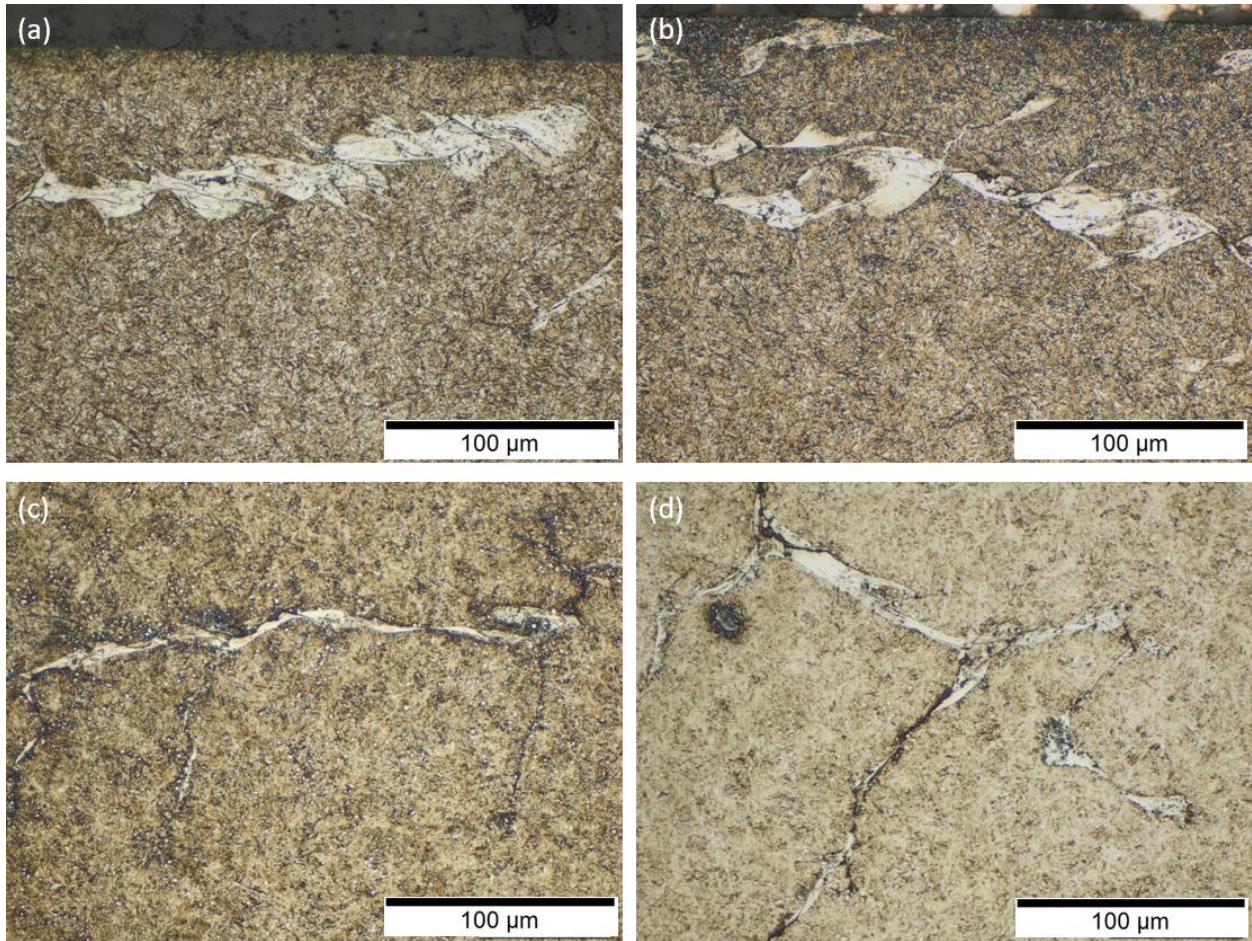


Figure 11. Four images illustrating that the carburized AISI 3310 samples (a) and (b), on average, were accompanied by much larger regions of microstructural alterations when compared to the through-hardened AISI 52100 samples (c) and (d) (the images are oriented so the raceway is at the top of the page and the over-rolling direction is from the left to the right)

5.0 Conclusions

Benchtop test samples were manufactured from two different steel alloys and hardened via two different heat treatment processes. One set of samples consisted of through-hardened AISI 52100 steel, and the other consisted of carburized AISI 3310 steel. Four samples from each set were tested under identical conditions using the PCS Instruments micro-pitting rig (MPR). The presented test conditions, in conjunction with particular lubricant formulations, have previously been shown to lead to the formation of crack networks containing adjacent microstructural alterations (commonly referred to as white etching cracks, or WECs) [9,24,39].

1. Under the presented test conditions, it was observed that the carburized samples lasted on average ~2.3 times longer than the through-hardened samples before resulting in the formation of a macro-pit. It is hypothesized that the increase in test time was due to the combination of the inherent compressive stress and increased toughness within the samples resulting from the carburization process.
2. The morphology of the WEC networks varied between the through-hardened and carburized groups. Firstly, the WECs documented in the through-hardened samples showed multiple instance of vertical crack propagation spanning hundreds of microns into the subsurface, the WECs documented in the carburized samples show no such vertical propagation. Secondly, the white etching areas (WEAs) within the carburized samples were larger in comparison with those observed in the through-hardened samples. Both of these observations were attributed to the compressive residual stress inherent in the carburization process.
3. Additional tests were conducted that aimed to identify when WECs initiated in both steels. No significant difference in time to crack initiation could be documented. This suggests that the increase in time until a WEC induced macro-pit documented in the carburized samples was largely due to the prolonging of the propagation stage of damage formation. This can again be attributed to the significant compressive residual stress induced by the carburization process.

6.0 References

- [1] M.N. Kotzalas, G.L. Doll, Tribological advancements for reliable wind turbine performance, *Philos. Trans. R. Soc. Lond. Math. Phys. Eng. Sci.* 368 (2010) 4829–4850.
- [2] W. Musial, S. Butterfield, B. McNiff, Improving wind turbine gearbox reliability, in: *Eur. Wind Energy Conf. Milan Italy, 2007*: pp. 7–10. <http://www.mapcruzin.com/wind-power-publications/research-development/41548.pdf> (accessed June 16, 2015).
- [3] A. Greco, S. Sheng, J. Keller, A. Erdemir, Material wear and fatigue in wind turbine systems, *Wear*. 302 (2013) 1583–1591.
- [4] J.-H. Kang, B. Hosseinkhani, C.A. Williams, M.P. Moody, P.A.J. Bagot, P.E.J. Rivera-Díaz-del-Castillo, Solute redistribution in the nanocrystalline structure formed in bearing steels, *Scr. Mater.* 69 (2013) 630–633.
- [5] V. Šmeļova, A. Schwedt, L. Wang, W. Holweger, J. Mayer, Electron microscopy investigations of microstructural alterations due to classical Rolling Contact Fatigue (RCF) in martensitic AISI 52100 bearing steel, *Int. J. Fatigue*. 98 (2017) 142–154. doi:10.1016/j.ijfatigue.2017.01.035.
- [6] V. Šmeļova, A. Schwedt, L. Wang, W. Holweger, J. Mayer, Microstructural changes in White Etching Cracks (WECs) and their relationship with those in Dark Etching Region (DER) and White Etching Bands (WEBs) due to Rolling Contact Fatigue (RCF), *Int. J. Fatigue*. 100, Part 1 (2017) 148–158. doi:10.1016/j.ijfatigue.2017.03.027.
- [7] Y.-S. Su, S.-R. Yu, S.-X. Li, Y.-N. He, Review of the damage mechanism in wind turbine gearbox bearings under rolling contact fatigue, *Front. Mech. Eng.* (2017) 1–8. doi:10.1007/s11465-018-0474-1.
- [8] Y.-S. Su, S.-X. Li, S.-Y. Lu, X.-D. Shu, Deformation-induced amorphization and austenitization in white etching area of a martensite bearing steel under rolling contact fatigue, *Int. J. Fatigue*. 105 (2017) 160–168. doi:10.1016/j.ijfatigue.2017.08.022.
- [9] B. Gould, A. Greco, The Influence of Sliding and Contact Severity on the Generation of White Etching Cracks, *Tribol. Lett.* 60 (2015) 1–13.
- [10] A. Grabulov, R. Petrov, H.W. Zandbergen, EBSD investigation of the crack initiation and TEM/FIB analyses of the microstructural changes around the cracks formed under Rolling Contact Fatigue (RCF), *Int. J. Fatigue*. 32 (2010) 576–583.
- [11] A. Grabulov, U. Ziese, H.W. Zandbergen, TEM/SEM investigation of microstructural changes within the white etching area under rolling contact fatigue and 3-D crack reconstruction by focused ion beam, *Scr. Mater.* 57 (2007) 635–638.
- [12] J.A. Martin, S.F. Borgese, A.D. Eberhardt, Microstructural alterations of rolling—bearing steel undergoing cyclic stressing, *J. Fluids Eng.* 88 (1966) 555–565.
- [13] J.L. O’Brien, A.H. King, Electron microscopy of stress-induced structural alterations near inclusions in bearing steels, *J. Fluids Eng.* 88 (1966) 568–571.
- [14] T.B. Lund, J. Beswick, S.W. Dean, Sub-Surface Initiated Rolling Contact Fatigue—Influence of Non-Metallic Inclusions, Processing History, and Operating Conditions, *J. ASTM Int.* 7 (2010) 102559. doi:10.1520/JAI102559.
- [15] D. Scott, B. Loy, G.H. Mills, Paper 10: Metallurgical Aspects of Rolling Contact Fatigue, in: *Proc. Inst. Mech. Eng. Conf. Proc.*, SAGE Publications, 1966: pp. 94–103. <http://pcp.sagepub.com/content/181/15/94.short> (accessed July 20, 2015).
- [16] K. Stadler, J. Lai, R. Vegter, A Review: The Dilemma With Premature White Etching Crack (WEC) Bearing Failures, in: *Bear. Steel Technol.* 10th Vol. Adv. Steel Technol. Roll.

Bear., ASTM International, 2015.

http://www.astm.org/DIGITAL_LIBRARY/STP/PAGES/STP158020140046.htm (accessed April 11, 2016).

- [17] M.-H. Evans, An updated review: white etching cracks (WECs) and axial cracks in wind turbine gearbox bearings, *Mater. Sci. Technol.* (2016) 1–37.
- [18] J. Luyckx, Hammering Wear Impact Fatigue Hypothesis WEC/irWEA failure mode on roller bearings, (2011). http://www.nrel.gov/wind/pdfs/day2_sessioniv_3_hansen_luyckx.pdf.
- [19] S. Hyde, White Etch Areas: Metallurgical Characterization & Atomistic Modeling, (2014). <https://anl.app.box.com/s/hu1qs2y4tyfhg034bus2poiqlsalvu0h>.
- [20] W. Solano-Alvarez, H. Bhadeshia, White-etching matter in bearing steel. Part II: distinguishing cause and effect in bearing steel failure, *Metall. Mater. Trans. A.* 45 (2014) 4916–4931.
- [21] H. Bhadeshia, Steels for bearings, *Prog. Mater. Sci.* 57 (2012) 268–435.
- [22] M.-H. Evans, A.D. Richardson, L. Wang, R.J.K. Wood, Serial sectioning investigation of butterfly and white etching crack (WEC) formation in wind turbine gearbox bearings, *Wear.* 302 (2013) 1573–1582.
- [23] T. Bruce, E. Rounding, H. Long, R.S. Dwyer-Joyce, Characterisation of white etching crack damage in wind turbine gearbox bearings, *Wear.* 338 (2015) 164–177.
- [24] B. Gould, A. Greco, Investigating the Process of White Etching Crack Initiation in Bearing Steel, *Tribol. Lett.* 62 (2016) 1–14.
- [25] R. Errichello, S. Sheng, J. Keller, A. Greco, Wind Turbine Tribology: A Recap, U.S. Department of Energy, EERE Wind and Water Power Program, n.d. <http://www.nrel.gov/docs/fy12osti/53754.pdf>.
- [26] W. Holweger, Progresses in solving White etching crack phenomena, NREL-Gearbox Reliab. Collab. Gold. Colo. (2014) 45.
- [27] I. Strandell, C. Fajers, T. Lund, Corrosion—One Root Cause for Premature Failures, in: 37th Leeds-Lyon Symp. Tribol., 2010.
- [28] J. Loos, I. Bergmann, M. Goss, Influence of Currents from Electrostatic Charges on WEC Formation in Rolling Bearings, *Tribol. Trans.* 59 (2016) 865–875. doi:10.1080/10402004.2015.1118582.
- [29] J. Gegner, Tribological aspects of rolling bearing failures, INTECH Open Access Publisher, 2011.
- [30] B.J. Gould, D.L. Burris, Effects of wind shear on wind turbine rotor loads and planetary bearing reliability, *Wind Energy.* 19 (2015) 1011–1021. doi:10.1002/we.1879.
- [31] N. Garabedian, B. Gould, G. Doll, D. Burris, Wear and fatigue as contributors to the premature failure of wind turbine planet bearings - under-loading or over-loading?, *Tribol. Trans.* (2018). doi:10.1080/10402004.2018.1433345.
- [32] F. Gutiérrez Guzmán, M. Oezel, G. Jacobs, G. Burghardt, C. Broeckmann, T. Janitzky, Reproduction of white etching cracks under rolling contact loading on thrust bearing and two-disc test rigs, *Wear.* 390–391 (2017) 23–32. doi:10.1016/j.wear.2017.06.020.
- [33] H.K. Danielsen, F.G. Guzmán, K.V. Dahl, Y.J. Li, J. Wu, G. Jacobs, G. Burghardt, S. Fæster, H. Alimadadi, S. Goto, D. Raabe, R. Petrov, Multiscale characterization of White Etching Cracks (WEC) in a 100Cr6 bearing from a thrust bearing test rig, *Wear.* 370–371 (2017) 73–82. doi:10.1016/j.wear.2016.11.016.

- [34] A.D. Richardson, M.-H. Evans, L. Wang, R.J.K. Wood, M. Ingram, B. Meuth, The Evolution of White Etching Cracks (WECs) in Rolling Contact Fatigue-Tested 100Cr6 Steel, *Tribol. Lett.* 66 (2018) 6. doi:10.1007/s11249-017-0946-1.
- [35] A.D. Richardson, M.-H. Evans, L. Wang, R.J.K. Wood, M. Ingram, Thermal Desorption Analysis of Hydrogen in Non-hydrogen-Charged Rolling Contact Fatigue-Tested 100Cr6 Steel, *Tribol. Lett.* 66 (2018) 4. doi:10.1007/s11249-017-0947-0.
- [36] M. Scepanskis, B. Gould, A. Greco, Empirical Investigation of Electricity Self-Generation in a Lubricated Sliding–Rolling Contact, *Tribol. Lett.* 65 (n.d.) 109–119.
- [37] M.-H. Evans, A.D. Richardson, L. Wang, R.J.K. Wood, W.B. Anderson, Confirming subsurface initiation at non-metallic inclusions as one mechanism for white etching crack (WEC) formation, *Tribol. Int.* 75 (2014) 87–97.
- [38] J. Franke, J.T. Carey, S. Korres, T. Haque, P.W. Jacobs, J. Loos, W. Kruhoeffler, White Etching Cracking—Simulation in Bearing Rig and Bench Tests, *Tribol. Trans.* 0 (2017) 1–11. doi:10.1080/10402004.2017.1339839.
- [39] B. Gould, N.G. Demas, G. Pollard, J.J. Rydel, M. Ingram, A.C. Greco, The Effect of Lubricant Composition on White Etching Crack Failures, *Tribol. Lett.* 67 (2018) 7. doi:10.1007/s11249-018-1106-y.
- [40] A.D. Richardson, M.-H. Evans, L. Wang, M. Ingram, Z. Rowland, G. Llanos, R.J.K. Wood, The effect of over-based calcium sulfonate detergent additives on white etching crack (WEC) formation in rolling contact fatigue tested 100Cr6 steel, *Tribol. Int.* 133 (2019) 246–262. doi:10.1016/j.triboint.2019.01.005.
- [41] F. Manieri, K. Stadler, G.E. Morales-Espejel, A. Kadiric, The origins of white etching cracks and their significance to rolling bearing failures, *Int. J. Fatigue.* 120 (2019) 107–133. doi:10.1016/j.ijfatigue.2018.10.023.
- [42] K. Iso, A. Yokouchi, H. Takemura, Research work for clarifying the mechanism of white structure flaking and extending the life of bearings, SAE Technical Paper, 2005. <http://papers.sae.org/2005-01-1868/> (accessed June 16, 2015).
- [43] R.H. Vegter, J.T. Slycke, The role of hydrogen on rolling contact fatigue response of rolling element bearings, *J. ASTM Int.* 7 (2009) 1–12.
- [44] H. Uyama, H. Yamada, H. Hidaka, N. Mitamura, The effects of hydrogen on microstructural change and surface originated flaking in rolling contact fatigue, *Tribol. Online.* 6 (2011) 123–132.
- [45] K. Hiraoka, T. Fujimatsu, N. Tsunekage, A. Yamamoto, Generation process observation of micro-structural change in rolling contact fatigue by hydrogen-charged specimens, *J. Jpn. Soc. Tribol.* 52 (2007) 888–895.
- [46] N. Kino, K. Otani, The influence of hydrogen on rolling contact fatigue life and its improvement, *JSAE Rev.* 24 (2003) 289–294.
- [47] K. Tamada, H. Tanaka, Occurrence of brittle flaking on bearings used for automotive electrical instruments and auxiliary devices, *Wear.* 199 (1996) 245–252.
- [48] J.A. Ciruna, H.J. Szieleit, The effect of hydrogen on the rolling contact fatigue life of AISI 52100 and 440C steel balls, *Wear.* 24 (1973) 107–118.
- [49] L. Grunberg, The formation of hydrogen peroxide on fresh metal surfaces, *Proc. Phys. Soc. Sect. B.* 66 (1953) 153.
- [50] T. Imran, B. Jacobson, A. Shariff, Quantifying diffused hydrogen in AISI-52100 bearing steel and in silver steel under tribo-mechanical action: Pure rotating bending, sliding–rotating bending, rolling–rotating bending and uni-axial tensile loading, *Wear.* 261 (2006) 86–95.

- [51] D. Ray, L. Vincent, B. Coquillet, P. Guirandeny, J. Chene, M. Aucouturier, Hydrogen embrittlement of a stainless ball bearing steel, *Wear*. 65 (1980) 103–111.
- [52] Y. Matsubara, H. Hamada, A novel method to evaluate the influence of hydrogen on fatigue properties of high strength steels, *J ASTM Int*. 3 (2006) 1–14.
- [53] H. Lü, M. Li, T. Zhang, W. Chu, Hydrogen-enhanced dislocation emission, motion and nucleation of hydrogen-induced cracking for steel, *Sci. China Ser. E Technol. Sci.* 40 (1997) 530–538.
- [54] S. Fujita, S. Matsuoka, Y. Murakami, G. Marquis, Effect of hydrogen on mode II fatigue crack behavior of tempered bearing steel and microstructural changes, *Int. J. Fatigue*. 32 (2010) 943–951.
- [55] M.-H. Evans, A.D. Richardson, L. Wang, R.J.K. Wood, Effect of hydrogen on butterfly and white etching crack (WEC) formation under rolling contact fatigue (RCF), *Wear*. 306 (2013) 226–241.
- [56] A. Ruellan, F. Ville, X. Kleber, A. Arnaudon, D. Girodin, Understanding white etching cracks in rolling element bearings: The effect of hydrogen charging on the formation mechanisms, *Proc. Inst. Mech. Eng. Part J J. Eng. Tribol.* 228 (2014) 1252–1265.
- [57] M.-H. Evans, L. Wang, H. Jones, R.J.K. Wood, White etching crack (WEC) investigation by serial sectioning, focused ion beam and 3-D crack modelling, *Tribol. Int.* 65 (2013) 146–160.
- [58] M. Paladugu, R. Scott Hyde, White etching matter promoted by intergranular embrittlement, *Scr. Mater.* 130 (2017) 219–222. doi:10.1016/j.scriptamat.2016.11.030.
- [59] M. Paladugu, S. Hyde, Microstructure deformation and white etching matter formation along cracks, *Wear*. 390–391 (2017) 367–375.
- [60] S.-X. Li, Y.-S. Su, X.-D. Shu, J.-J. Chen, Microstructural evolution in bearing steel under rolling contact fatigue, *Wear*. 380–381 (2017) 146–153. doi:10.1016/j.wear.2017.03.018.
- [61] T. Bruce, H. Long, T. Slatter, R. s. Dwyer-Joyce, Formation of white etching cracks at manganese sulfide (MnS) inclusions in bearing steel due to hammering impact loading, *Wind Energy*. 19 (2016) 1903–1915. doi:10.1002/we.1958.
- [62] B. Gould, A. Greco, K. Stadler, X. Xiao, An analysis of premature cracking associated with microstructural alterations in an AISI 52100 failed wind turbine bearing using X-ray tomography, *Mater. Des.* 117 (2017) 417–429. doi:10.1016/j.matdes.2016.12.089.
- [63] K. Stadler, R. Vegter, D. Vaes, White etching cracks, *Evol. Online*. (n.d.). <http://evolution.skf.com/us/white-etching-cracks-a-consequence-not-a-root-cause-of-bearing-failure/>.
- [64] B. Gould, A. Greco, K. Stadler, E. Vegter, X. Xiao, Using advanced tomography techniques to investigate the development of White Etching Cracks in a prematurely failed field bearing, *Tribol. Int.* (2017). doi:10.1016/j.triboint.2017.07.028.
- [65] Y. Shen, S.M. Moghadam, F. Sadeghi, K. Paulson, R.W. Trice, Effect of retained austenite – Compressive residual stresses on rolling contact fatigue life of carburized AISI 8620 steel, *Int. J. Fatigue*. 75 (2015) 135–144. doi:10.1016/j.ijfatigue.2015.02.017.
- [66] D.K. Matlock, K.A. Alogab, M.D. Richards, J.G. Speer, Surface processing to improve the fatigue resistance of advanced bar steels for automotive applications, *Mater. Res.* 8 (2005) 453–459. doi:10.1590/S1516-14392005000400017.
- [67] G. Krauss, Chapter 21, in: *Steels Process. Struct. Perform.*, ASM International, 2015.
- [68] R. Errichello, R. Budny, R. Eckert, Investigations of bearing failures associated with white etching areas (WEAs) in wind turbine gearboxes, *Tribol. Trans.* 56 (2013) 1069–1076.

- [69] ASTM E975-03 Standard Practice for X-Ray Determination of Retained Austenite in Steel with Near Random Crystallographic Orientation, (n.d.).
- [70] ASTM E2860-12 Standard Test Method for Residual Stress Measurements by X-Ray Diffraction for Bearing Steels, (2012).
- [71] M.-H. Evans, A.D. Richardson, L. Wang, R.J.K. Wood, W.B. Anderson, Confirming subsurface initiation at non-metallic inclusions as one mechanism for white etching crack (WEC) formation, *Tribol. Int.* 75 (2014) 87–97.
- [72] Richardson, A. D., Investigation of White Etching Crack (WEC) formation mechanisms under non-hydrogen charged test conditions, (2014).
- [73] J. Brändlein, P. Eschmann, L. Hasbargen, K. Weigand, *Ball and roller bearings: theory, design and application*, Third Edition, Wiley, 1999.
- [74] D. Girodin, *Deep Nitrided 32CrMoV13 Steel*, n.d.
- [75] H. Singh, R.V. Pulikollu, W. Hawkins, G. Smith, Investigation of Microstructural Alterations in Low- and High-Speed Intermediate-Stage Wind Turbine Gearbox Bearings, *Tribol. Lett.* 65 (2017) 81. doi:10.1007/s11249-017-0861-5.
- [76] M.H. Evans, White structure flaking (WSF) in wind turbine gearbox bearings: effects of 'butterflies' and white etching cracks (WECs), *Mater. Sci. Technol.* 28 (2012) 3–22.